The Construction of Two-Dimensional Potential Energy Surfaces of Reactions with Post-Transition State Bifurcations

Hsiao-Han Chuang,[†,‡,§] Dean J. Tantillo,[*,¶] and Chao-Ping Hsu[*,‡]

†*Department of Chemistry, National Taiwan University, Taipei, Taiwan*

‡*Institute of Chemistry, Academia Sinica, Taipei, Taiwan*

¶*Department of Chemistry, University of California-Davis, Davis, CA USA*

§*Nanoscience and Technology Program, Taiwan International Graduate Program, Academia Sinica and National Taiwan University*

E-mail: djtantillo@ucdavis.edu; cherri@sinica.edu.tw

Abstract

Reactions with post-transition state bifurcations (PTSBs) involve an initial ambimodal transition-state structures followed by an unstable region leading to two possible products. PTSBs are seen in many organic, organometallic and biosynthetic reactions, but analyzing the origins of selectivity for these reactions is challenging, in large part due to the complex nature of the potential energy surfaces involved, which precludes analyses based on single intrinsic reaction path (IRP). While selectivity can be predicted using molecular dynamics simulation, connecting results from such calculations to the topography of potential energy surfaces is difficult. In the present work, a method for generating two-dimensional potential energy surfaces for PTSBs is described. The first dimension starts with the IRP for the first transition-state structure, followed by a modified reaction coordinate that reaches the second transition-state structure, which

interconverts the two products of a bifurcating reaction path. The IRP for the second transition-state structure constitutes the second dimension. In addition, a method for mapping trajectories from Born-Oppenheimer molecular dynamics simulations onto these surfaces is described. Both approaches are illustrated with representative examples from the field of organic chemistry. The 2D-PESs for five asymmetric cases tested have clear tilted topography after the first transition-state structure, and tilted direction correlate well with the selectivity observed from previous dynamic simulation. Instead of selecting reaction coordinates by chemical intuition, our method provides a general means to construct two-dimensional potential energy surfaces for reactions with post-transition state bifurcations.

1 Introduction

A reaction with a post-transition state bifurcation (PTSB) is a reaction starting from a single transition-state structure (TSS) that leads to two products without any intervening potential energy surface (PES) minima.[1,2] With PTSB, it is no longer possible to predict the reaction through the canonical transition-state theory,[3,4] nor the kinetic controlled products since the activation energy for the two products are identical. The selectivity of a variety of reactions — organic, organometallic, biosynthetic — leading to complex organic molecules[5–7] has been shown to depend on non-statistical dynamic effects[8,9] that influence trajectories as they approach the region of a PES containing a bifurcation.

Various means of characterizing PESs with unusual features have been discussed in the literature.[1] Here we highlight some of those most relevant to PESs and reaction paths with PTSBs. Kraka extended the idea of a reaction path Hamiltonian (i.e., searching reaction path with contributions from different normal modes) from Miller[10] to use curvature coupling to recognize 'hidden intermediates' of symmetry forbidden pericyclic reactions with PTSBs[11–13] Quapp redefined the concept of reaction path following a reduced gradient (RGF) method, which he used to calculate bifurcating paths,[14] and the tangent search concept (TASC)

method, which he used to calculate valley extremal.[15] Gill implemented an algorithm to locate branching points by justifying the change of curvature.[16] Wales used gradient lines to build two-dimensional potential energy surfaces (2D-PESs) for symmetric PTSBs.[17] Following up on Maeda's automatic search method, the artificial force induced reaction (AFIR) methods[18] minimize the so-called 'AFIR function' to search for stationary points, and the difficulty of this approach in connecting PTSBs via intrinsic reaction coordinates is also discussed.[19] Taketsugu proposed an approach that uses the classical multidimensional scaling (CMDS) method[20] to reduce the dimensionality of data sets, allowing for interpretation of multiple IRPs using low-dimensional representations.

Investigation of PTSBs is intrinsically a multi-dimensional problem;[21] at least two degrees-of-freedom (d.o.f.) are needed. Consequently, it is difficult to describe reactions with PTSBs using traditional one-dimensional pictures such as minimum-energy paths[22] or intrinsic reaction paths/coordinates (IRP/IRC).[23] Quapp[24] explicitly addressed the fact that the solution of IRP is unique and there cannot be a bifurcation on gradient lines. In recent work, Hare and co-workers developed a method to determine important structural changes during reactions using principle component analysis with their program *PathReducer*.[25] The method we describe here is complementary to these approaches, in that it does not reduce dimensionality by focusing on a subset of the structural changes that occur during a reaction, but rather reduces dimensionality by focusing on the IRPs for the initial, pre-PTSB TSS and a secondary TSS that intercoverts the two products.

In investigating selectivity of organic reactions with PTSBs, 'pitchfork model' are widely discussed.[1,26–30] The key features of this model are shown in Figure 1. A reactant (**R**) connects to the first transition-state structure (**TSS1**), which is referred to as 'ambimodal'[31] which is followed by a descending valley that leads to an *orthogonal* ridge connecting to a second transition-state structure (**TSS2**) that interconverts the two products (**P1** and **P2**). In addition to these stationary points, the path from the valley following **TSS1** toward the **TSS2** ridge has a valley-ridge inflection (**VRI**) point.[24,32–34] The overall reaction path (not

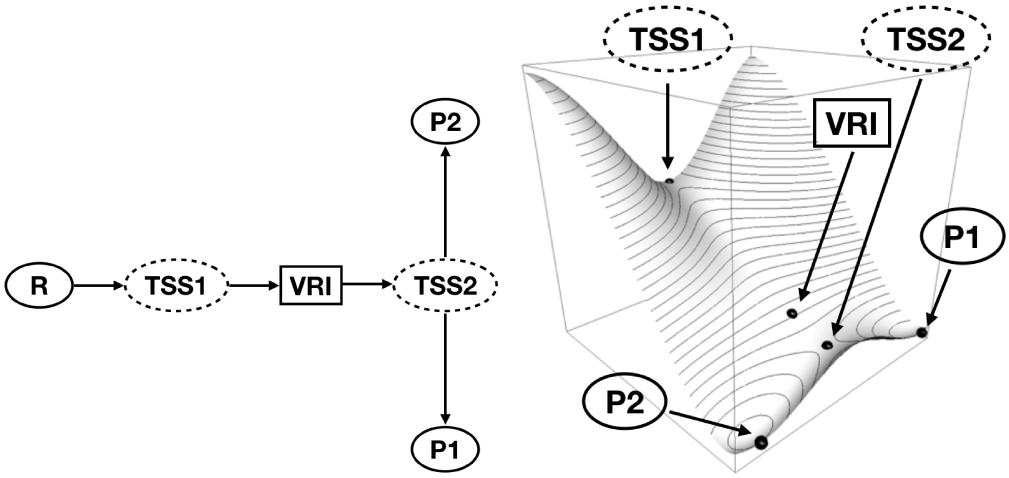

(a) (b)

Figure 1: The pitchfork model has six important points which include five stationary points and one non-stationary point, as listed in (a) solid ovals represent three local minima and dashed ovals represent two TSSs. The non-stationary point is called valley-ridge inflection (**VRI**) point as is represented by a solid rectangle. In panel (b), a three-dimensional view from the products side is illustrated (see Appendix of Ref. 24).

.

necessarily the path followed by dynamics trajectories, *vide infra*) can be represented as **R** $\rightarrow$ **TSS1** $\rightarrow$ **VRI** $\rightarrow$ **TSS2** $\rightarrow$ **P1**/**P2**.

The presence of a **VRI** causes a locally flat region that separates the valley that immediately follows the TSS and the ridge that separates two products. A **VRI**[24] has at least one eigenvalue of the Hessian (**H**) that is zero ; $\mathbf{H}\mathbf{v}_{\mathrm{VRI}} = 0$, and this gradient ($\mathbf{g}_{\mathrm{VRI}}$) is orthogonal to the corresponding zero Hessian eigenvector ($\mathbf{L}_{\mathrm{VRI}}$); $\mathbf{g}_{\mathrm{VRI}}^{\mathrm{T}} \cdot \mathbf{L}_{\mathrm{VRI}} = 0$. Two types of **VRI** points are discussed in the literature: symmetric **VRI** points[33] and asymmetric **VRI** points,[35] which leads to symmetric PTSB and asymmetric PTSB, and their conceptual difference of topography are shown in Figure 2.

2D-PESs for symmetric PTSB have been constructed, but only for small systems by using selected geometric parameters (e.g. distances, bond angles, dihedral angles or collective variables in which some of these are combined),[27,29,34,36] or using two gradient lines.[37] Using geometric parameters is inherently biases by chemists' (pre)conceptions of which structural parameters are most important. In a PES of a symmetric PTSB, as shown in panel (a) of

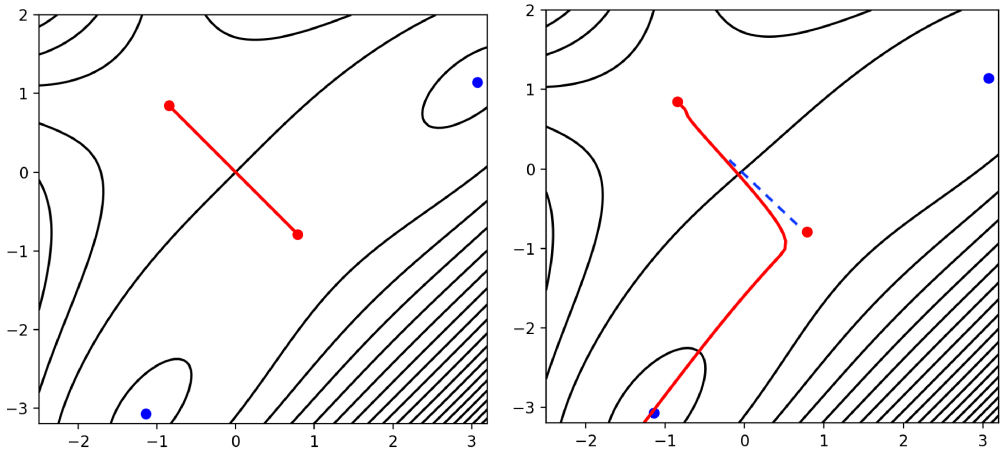

(a) (b)

Figure 2: Pitchfork model potential for symmetric (a) and asymmetric (b) PTSBs are shown in their important bifurcated region (similar to Figure 1 (b)). Red and blue points are local maxima and minima, respectively. Steepest descent path is the red solid line, and blue dash line is the artificial reaction path. The analytical function is $E(x,y) = \frac{1}{2}(xy^2 - yx^2 - \mu x + 2y) + \frac{1}{30}(x^4 + y^4)$,[35] and μ is 2.0 for symmetric (a) and 1.75 for asymmetric (b) PTSBs.

Figure 2, the reaction coordinate corresponding to **TSS1** is orthogonal to that for **TSS2**, and the IRP for **TSS1** terminates at **TSS2**. Baker referred to a TSS at which an IRP terminates as a 'false minimum',[16] which is similar to Kraka's 'hidden transition state' concept.[12] As will be shown in the present work, the two orthogonal IRPs can be used to construct a 2D-PES for further studies. In any case, dynamics trajectories for a symmetric 2D-PES are expected to be evenly distribute between both **P1** and **P2**, i.e., such a reaction displays no selectivity.

In contrast, reactions involving asymmetric PTSB are more general , and the prediction for selectivity has been difficult, which has led to sustained interest in their 2D-PESs.[1,2,30] The first asymmetric PTSB for real molecule is a reaction mechanism of ketyl anion radical anions in 1997.[38] Selectivity for a reaction with a PTSB associated with an asymmetric **VRI** cannot be described/predicted by canonical transition-state theory,[39] since it depends on the nature of the PES after passing the first transition-state structure.[40] As shown in panel (b) of Figure 2, the red solid line of IRP starts at **TSS1** and then goes to either **P1** or **P2** without reaching **TSS2**. Generally this IRP contains a shoulder near a **VRI**

point in 1D energy profile, and the shoulder have been taken as potential markers of the presence of PTSBs[41,42] and are related to the concept of 'hidden intermediates'.[12,43] The tilted topography of the 2D-PES on the product side of **TSS1** is associated with unequal probabilities of forming products **P1** and **P2** in dynamics trajectories, i.e., selectivity can be expected from a 2D-PES. Therefore it is important to develop strategies to build the 2D-PES for a general class of systems.

Our approach to building an asymmetric 2D-PES builds on the work of Minyaev and Wales.[17] Since an IRP for a reaction with an asymmetric PTSB does not reach **TSS2**, it does not fully capture the **VRI** and post-VRI region. Nonethless, IRPs may be used as ingredients to construct 2D-PESs for reactions with PTSBs. As discussed previously, a useful 2D map should contain two coordinates: one for the reaction where bifurcation would occur, and another direction for spanning the two bifurcation products.[44] By analyzing the gradient for these two reaction coordinates, each associated with an IRP, we define an artificial reaction coordinate to bridge the gap between **VRI** and **TSS2**, as shown in panel (b) of Figure 2 (blue dashed lines).

In Section 2, we briefly review normal mode analysis and its extension to IRPs. Conceptual applications to two subcategories of PTSB - containing systems are presented: symmetric systems in which normal IRPs are used to build a 2D-PES (Section 2.1) and asymmetric systems in which a modified reaction coordinate is defined (Section 2.2). An approach based on use of root-mean-square-deviation (RMSD) to map dynamics trajectories onto these numerical PESs is then described (Section 2.3). Chemical applications of the above methods are shown in Section 3, followed by a discussion of directions for future work in Section 4.

2 Methodology

In this section, we first review normal mode analysis and the development of an approach that combines IRPs to investigate PTSBs is laid out in Section 2.1 and 2.2.

In the normal mode analysis,[45] the potential (V) is expanded near the equilibrium geometry (q_{eq}, such that $V(q_{eq}) = V_0$) in mass-weighted coordinates to the second order,

$$V = V_0 + \frac{1}{2}\mathbf{q}^\intercal \mathbf{H} \mathbf{q}, \tag{1}$$

where $\mathbf{q}$ is a vector containing small displacements in the same reference frame, such that $\mathbf{q} = (\sqrt{m_1}\Delta x_1, \sqrt{m_1}\Delta y_1, \sqrt{m_1}\Delta z_1 \dots)$, with $\Delta x_i = x_i - x_{eq,i}$. $\mathbf{H}$ is the Hessian matrix (the second-order derivatives) evaluated at V_0.

$$H_{ij} = \left.\frac{\partial^2 V}{\partial q_i \partial q_j}\right|_{\mathbf{q}=0} \tag{2}$$

Since the Hessian is a symmetric matrix, we can diagonalize it with a set of orthogonal eigenvectors, and with real eigenvalues obtained:

$$\mathbf{H} = \mathbf{P}^\intercal \mathbf{D} \mathbf{P}, \tag{3}$$

where $\mathbf{D}$ is its diagonal eigenvalue matrix, $D_{ij} = \lambda_i \delta_{ij}$, with matrix element $\{\lambda_i\}$ being the eigenvalues. $\mathbf{P}$ ($\mathbf{P} = \mathbf{L}\mathbf{L}^\intercal$) is a matrix composed of columns of the eigenvectors of $\mathbf{H}$. From Eq. (3), we can obtain Eq. (1) as

$$\begin{aligned} V &= V_0 + \frac{1}{2}\mathbf{q}^\intercal(\mathbf{P}^\intercal \mathbf{D} \mathbf{P})\mathbf{q} && (4)\\ &= V_0 + \frac{1}{2}(\mathbf{q}^\intercal \mathbf{P}^\intercal)\mathbf{D}(\mathbf{P}\mathbf{q}) && (5)\\ &= V_0 + \frac{1}{2}\mathbf{Q}^\intercal \mathbf{D} \mathbf{Q} && (6)\\ &= V_0 + \sum_{i=1}^{3N} \frac{1}{2}\lambda_i Q_i^2 && (7) \end{aligned}$$

The new coordinates $\mathbf{Q}(\equiv \mathbf{P}\mathbf{q})$ correspond to the projection of atomic positions given by the Hessian eigenvectors, which are the *normal coordinates*, Q_i and $i = 1, 2, \cdots 3N$. In this coordinate, the collective motion of all of the atoms is included.

To define a reaction path, the most common approach uses steepest-descent path in mass-weighted coordinates.[23] This reaction coordinate is called intrinsic reaction coordinate (IRC) and the corresponding reaction path is intrinsic reaction path (IRP). Its mathematically definition is

$$\frac{d\mathbf{x}^{\mathrm{IRP}}(s)}{ds} = -\frac{\mathbf{G}[\mathbf{x}(s)]}{\parallel \mathbf{G}[\mathbf{x}(s)] \parallel} \tag{8}$$

$\mathbf{x}^{\mathrm{IRP}}$ has s as arc length and $\mathbf{G}$ as its gradient. It is an initial value problem[32] that requires a set of initial value to solve. However, when we start from a TSS for finding its corresponding reaction path, it has a null gradient initially and Eq. (8) would not propagate. Therefore, the initial step is usually replaced by the Hessian eigenvector, $\mathbf{L}_1$, with an negative eigenvalue, scaled by a small positive or negative factor, and the reaction path is now moved towards the one of the two convex directions of the TSS initially. The path $\mathbf{x}^{\mathrm{IRP}}$ is then propagated by the nonzero gradient subsequently, until zero gradient is reached, a potential minimum point in most cases that represent reactant or product of this TSS.

2.1 2D-PES of special cases: symmetric PTSBs

For reactions with symmetric PTSBs, the IRP of **TSS1** terminates at **TSS2**, the molecular structure has nuclear symmetry and the IRP for **TSS2** is symmetric.[46] The eigenvectors with one and only one negative eigenvalue for **TSS1** and **TSS2** are orthogonal to each other. Both **P1** and **P2** are chemically identical differing only if different atoms of the same type are numbered differently. Therefore, the 2D-PES is symmetric.

For a symmetric PTSB system, we first obtained the IRPs corresponding to **TSS1** and **TSS2**. We then build a symmetric 2D-PES with the following three steps. We first translate and rotate the structures of the IRP of **TSS1** if their orientations are different from the structures of the IRP of **TSS2**. For a 2D-PES, all the molecular geometries should refer to the same origin of Cartesian coordinates and aligned to the same orientation. However, for two independent outputs of electronic structure calculation, the orientation and the origin of

Cartesian coordinates of molecular structures may not be the same. Thus, if two IRPs have different origin and orientation, we rotate molecular structures via the Kabsch algorithm[47] followed by a translation. (c.f. Python and Fortran source code are given in the following GitHub URL, https://github.com/HHChuang/align2mole)

Second, we calculate the structural difference between two neighboring molecular structures along the IRP for **TSS2**.

Finally, in order to obtain the corresponding structure for the grids of 2D-PES, we shift all the structures in the IRP for **TSS1** by adding the above structure difference derived from the IRP of **TSS2**. With the structures defined in the 2-D array, the PES can be obtained with the calculated energy for each structure.

Therefore, the procedure we employed is:

1. Generate IRP for both TSSs. The IRP for **TSS1** leads to **TSS2**.
2. Align the structures of IRPs;
3. Calculate structures difference;
4. Generate structures on this symmetric 2D-PES grid and obtains the PES accordingly.

We note that our approach is similar to that of Wales,[17] and this method can only be applied to symmetric PTSBs.

2.2 2D-PES of general cases: asymmetric PTSBs

For reactions with asymmetric PTSBs, the above approach does not apply, as the IRP from **TSS1** will *not* leads to **TSS2**. Instead it leads to either **P1** or **P2** dependents on the PES of the system. The IRP following **TSS1** usually shows a shoulder, which is a characteristic near a **VRI** region.[1,48] At this region, we should aim to search for a path that ends at **TSS2**, instead of letting the IRP leading the path to **P1** or **P2**. Here, instead of locating the exact

position of **VRI** points, we simply stop the IRP near the region, and aim to find the path connection between **TSS1** and **TSS2**. We call this connection the *artificial reaction path*.

After reaching **VRI**, the major problem of IRP from **TSS1** is that it deviates from the ridge by following the gradient, reaching one of the products **P1** or **P2**. In order to reach **TSS2**, a strategy was developed such that the new reaction path follows the ridge.

Here we aim to modify Eq. (8) such that it follows the ridge without falling to the basin for **P1** or **P2**. In order to do so, we remove the projection of gradient $\mathbf{G}$ that is parallel to the first Hessian eigenvector of **TSS2** with a negative eigenvalue, $\mathbf{L}_1^{\mathbf{TSS2}}$, forming $\mathbf{G}^{\mathrm{ARP}}$.

$$\mathbf{G}^{\mathrm{ARP}} = \mathbf{G}^{\mathrm{original}} - \frac{\mathbf{G}^{\mathrm{original}} \cdot \mathbf{L}_1^{\mathbf{TSS2}}}{\|\mathbf{L}_1^{\mathbf{TSS2}}\|^2} \mathbf{L}_1^{\mathbf{TSS2}} \tag{9}$$

The artificial reaction path (ARP), $\mathbf{x}^{\mathrm{ARP}}$, is defined as

$$\frac{d\mathbf{x}^{\mathrm{ARP}}(s)}{ds} = -\frac{\mathbf{G}^{\mathrm{ARP}}[\mathbf{x}^{\mathrm{ARP}}(s)]}{\| \mathbf{G}^{\mathrm{ARP}}[\mathbf{x}^{\mathrm{ARP}}(s)] \|} \tag{10}$$

Therefore, for two given IRPs of **TSS1** and **TSS2**, we build a 2D-PES for these systems through the following processes:

First, from the IRP of **TSS1**, an initial point is manually selected near the presumed **VRI** region (i.e., the shoulder in the IRP for **TSS1**). The electronic energy of the selected point should larger than that of **TSS2**. We note that the structures of the two IRPs of **TSS1** and **TSS2** should also be aligned such that they have the same orientation (c.f. step 2 in Section 2.1). Next, the gradient of this point is modified according to Eq. (10), keeping the component that is perpendicular to $\mathbf{L}_1^{\mathbf{TSS2}}$.

In each iterative step, Eq. (10) is propagated by adding the modified gradient to the structure of the previous point, followed by another electronic structure calculation for the gradient for the next step, forming a series of structures representing the ARP.

Third, the iteration generates structures until the energy difference between the derivative molecule and **TSS2** is less than 10^{-4} hartree (which conforms to a chemical accuracy of $\leq$

1 kcal/mol).

Finally, a 2D-PES was build for general cases with two reaction coordinates. The first dimension is composed of part of the IRP for **TSS1**, combined with the ARP that leads to **TSS2**. The other dimension is the IRP for **TSS2**. Similar to the symmetric case, the structures on the 2D grid was generated by taking all the structures on the first dimension, and shifting by the structural difference on the second dimension, i.e., the difference between any point on the IRP of **TSS2**. In asymmetric cases, we have also optimized the structures on the 2D-PES along the the effect from other d.o.f. may deviate the 2D grid that we also optimized the structures of 2D-PES along modified gradients, where the modified gradients are the components of gradient which are perpendicular to this surface. In each grid point, we take its gradient from electronic structure calculation, and then subtract its component gradient along x direction (from **TSS1** to **TSS2**) and along y direction (from **P1** to **P2**) on this surface. After that, we shift structure along the remained gradient to perform constrained optimization.

The process is summarized as : (c.f. GitHub, https://github.com/HHChuang/2DPES_PTSB).

1. Select a point near **VRI** region from IRP of **TSS1**;
2. Starting from the point selected, obtain the modified gradient with Eq. (9), and proceed to generate a new structure in ARP.
3. Repeat step 2 until the energy converge to **TSS2**.
4. Generate structures on this asymmetric 2D-PES by combining the shift in the second dimension to the first dimension, and a constrained optimization.

2.3 BOMD trajectories and their mapping to 2D-PES

Trajectories were taken from Ref. 41, where they were calculated using the program *Progdyn* developed by Singleton[49] for *ab initio*, specifically Born-Oppenheimer, molecular dynamics[50,51] (BOMD). To capture rare chemical events, downhill dynamic trajectories were

perform that they start from **TSS1**. And then quasi-classical sampling[52] was employed such that the starting points at **TSS1** follows the Boltzmann distribution for a given temperature in their energies. The subsequent structures were generated using normal coordinates (Eq. (2.23) in Ref. 52). The trajectories were obtained with the Verlet algorithm in solving the classical equation-of-motion, with step size set to 1 fs in the present work.

A given dynamics trajectory involves time evolution of all d.o.f. It would be possible to better visualize the trajectories if we can map them onto the 2D-PESs (c.f. Section 2.1 and 2.2). To map structures along trajectories on to the 2D-PES, we first overlap the first point of a trajectory with the **TSS1** structure through translation and rotation. The translation overlaps the position of centriods. The rotation was performed via Kabsch algorithm.[47] The same rotation matrix applied to all subsequent points in the same trajectory.

Next, we use RMSD to locate the structures at each point of a trajectory on our 2D-PES.

$$\text{RMSD} = \sqrt{\frac{1}{N}\sum_{i=1}^{N}\left|\mathbf{a}_i^{\text{traj.}} - \mathbf{a}_i^{\text{2D-PES}}\right|^2}, \tag{11}$$

where N is the amount of atoms. The Cartesian coordinate of molecule is $\mathbf{a}_i$ with its x, y, and z component for atom i. $\mathbf{a}^{\text{traj.}}$ and $\mathbf{a}^{\text{2D-PES}}$ stand for the structure of trajectory and 2D-PES, respectively.

How to analyse trajectories to observe a meaningful physical picture is a difficult task. Here, we use RMSD of structure difference to map trajectories on a 2D-PES. Similar method to compare two distinct objects via a distance function to describe the jump between IRPs wes proposed before.[53]

For the first point of a trajectory, we compare its RMSD with all the structures on the 2D-PES grids and project it to the smallest RMSD, which is also the initial point for the trajectory. For the subsequent points, we compare its RMSD with an array of 7×7 grids on the PES, centering at the previous projection, and proceed with the smallest RMSD grid. This procedure is repeated iteratively until the end of the trajectory.

In addition, to improve resolution of trajectories without being constrained by the number of grid points of the 2D-PES, we search the minimum derivative of RMSD. Starting from the located coordinate from previous step, we search a unimodal area (i.e., only one extremum exists) in both the horizontal and vertical direction. After that, we use the Golden-section search method to locate the minimum derivative of RMSD.

2.4 Electronic structure calculations

All the electronic structure calculations described here were calculated using the GAUSSIAN09 program.[54] For the symmetric case described below, $H_3CO^{\bullet}$ isomerization, stationary points were optimized using MP2/6-31G(d,p), and the correlation energy was corrected by QCISD//MP2. The initial structure of **TSS1** was taken from the Figure 5 of Ref. 46, and **TSS2** was extracted form the last point of the IRP of **TSS1**, after constraining the symmetry to C_s. For the asymmetric cases described below, **NCH1** to **NCH5** (nomenclature used in Ref. 41 for consistency), the B3LYP density functional theory (DFT) method[55–59] was used with the 6-31+G(d,p) basis set. In order to obtain accurate eigenvectors, we added the **Freq=hpmodes** keywords in frequency calculations. Coordinates and energies for all the optimized structures are included in the Supporting information.

3 Results and discussion

Here we demonstrate our approach for constructing 2D-PES described in Section 2 with symmetric and asymmetric systems.

3.1 Symmetric PTSB: H_3CO isomerization

Methoxy radical isomerization ($H_3CO\cdot \rightarrow H_2C(\cdot)OH$) is one of the most widely studied reactions with a PTSB[16,26,29,46,60] (Scheme 1), the mechanism previously having been examined using both *ab initio* methods and DFT calculations on its electronic structure and symmetric

PES. In addition, wave packet dynamics simulations were also applied to this reaction.[29] We employ this system for a demonstration for our strategy in constructing a useful 2D-PES.

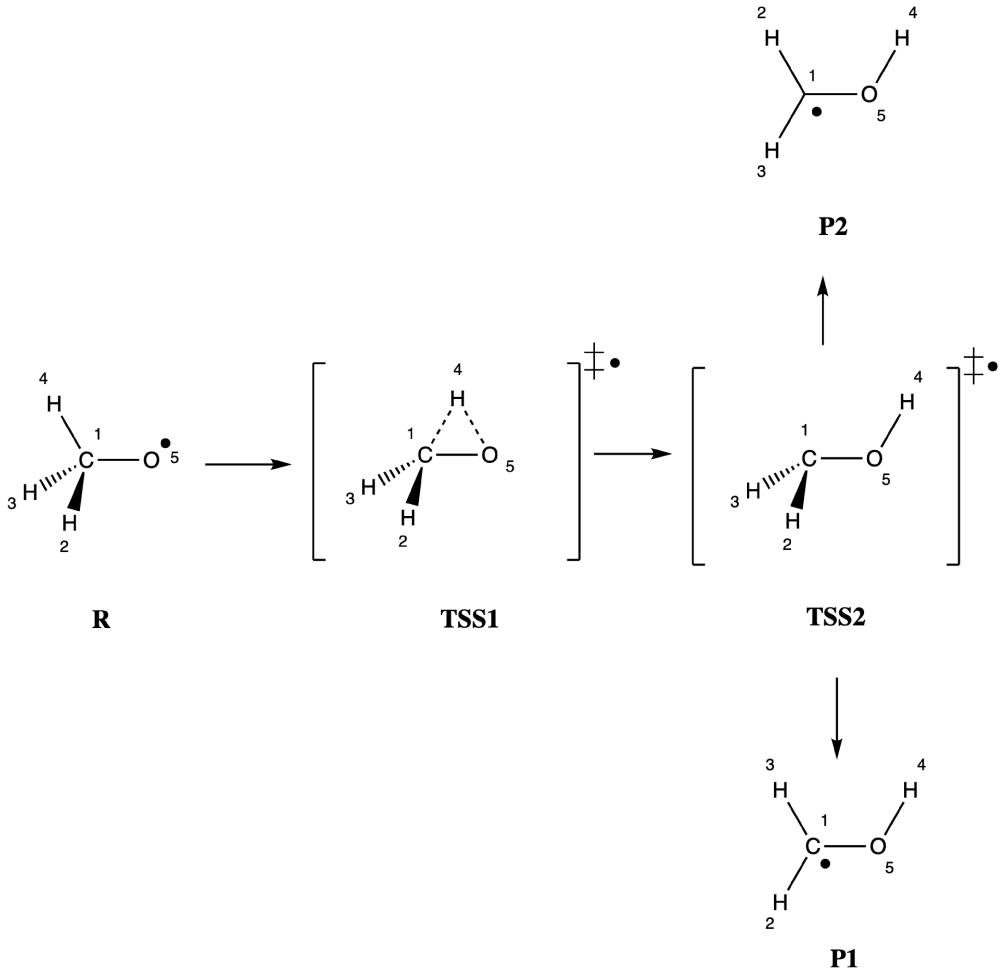

Scheme 1: Stationary points involved in methoxy radical isomerization.

The point group of fully optimized methoxy radical (**R**) is C_s rather than C_{3v} because of a Jahn-Teller distortion.[61] During the reaction in question, a hydrogen atom (H4)migrates to an oxygen atom (O5) via **TSS1**. The IRP from **TSS1** leads to the second TSS(**TSS2**; corresponding to rotation around the C−O bond) without any PES intermediate (**R**→**TSS1**→**TSS2**). Both **TSS1** and **TSS2** are of C_s symmetry, and thus, C_s symmetry is conserved along this path. We took the last point of this IRP as a new initial structure, re-optimized it and then found that it does have one and only one imaginary frequency.

However, by definition, if this reaction follows the minimum energy path, it will not reach

TSS2 and will instead go to either **P1** or **P2** (**R**→**TSS1**→**P1** or **P2**), if the initial point or the search of minimum energy path allows symmetry-breaking. Since in this case **P1** and **P2** are chemically identical, the difference between **P1** and **P2** is only in the atomic labels, i.e., which of H2 or H3 ends up near to C1. **P1** and **P2** are each C_s symmetric, but their symmetry elements are rotated with respect to those of **R**, **TSS1** and **TSS2**, and thus this pathway is a non-totally symmetric pathway, which is inconsistent with the Rodger-Schipper symmetry rules.[62] Taketsugu addresses this situation by noting that this non-totally symmetric path has no coupling to the totally symmetric path, which is an 'unstable intrinsic reaction path', i.e., it is a 'bifurcating reaction path'.[26,63]

Other than symmetry argument to justify a reaction with PTSB, existence of VRI point is another clue. VRI point is located between **TSS1** and **TSS2**, and it has two conditions; one is the small curvature, and the other is the orthogonality between its gradient and the corresponding Hessian eigenvector. We analyse the IRP between **TSS1** and **TSS2** at MP2 level. At point 0.47 $\sqrt{amu}Bohr$ (0.0 is the **TSS1**), its second normal mode has an imaginary frequency 78.61i cm^{-1}. Since the frequency is proportional to the square root of Hessian eigenvalue ($\omega_i \propto \sqrt{\lambda_i}$), and $\mathbf{H}^{\mathrm{VRI}}\mathbf{L}_2^{\mathrm{VRI}} = \lambda_2\mathbf{L}_2^{\mathrm{VRI}}$, thus, we can conclude that this point has a small curvature at the second normal mode. The second condition of orthogonality is also fulfilled that $(\mathbf{g}^{\mathrm{VRI}})^{\intercal}\mathbf{L}_2^{\mathrm{VRI}} = -1.53 \times 10^{-7}$. Above procedure is similar to Ref. 16.

Following the procedure described in Section 2.1, a 2D-PES for this reaction was built and shown in Figure 3. The horizontal axis corresponds to the IRP for **TSS1** and the vertical axis corresponds to the IRP of for **TSS2**. As expected, a symmetric surface with clear bifurcation character is obtained. Since the barrier associated with **TSS2** is approximately 2 kcal/mol, the PES near to it is almost flat at the scale of the Figure 3. Note that we did not symmetrize our surface; using the IRP allows us to capture this symmetry.

Since VRI position can be located in symmetric PTSB, we do one more test that $(\mathbf{L}_2^{\mathrm{VRI}})^{\intercal}\mathbf{L}_1^{\mathbf{TSS2}} = 0.99$ to show the parallel, where it is a good sign for extension of this method on asymmetric PTSB. In Eqn. (9), instead of decomposing gradient by its local

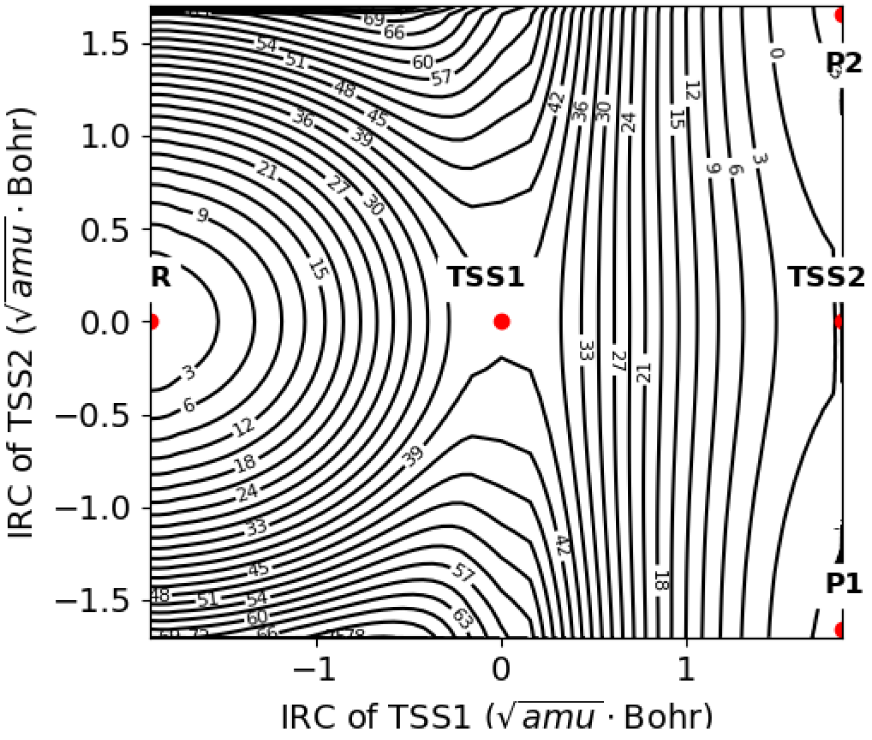

(a)

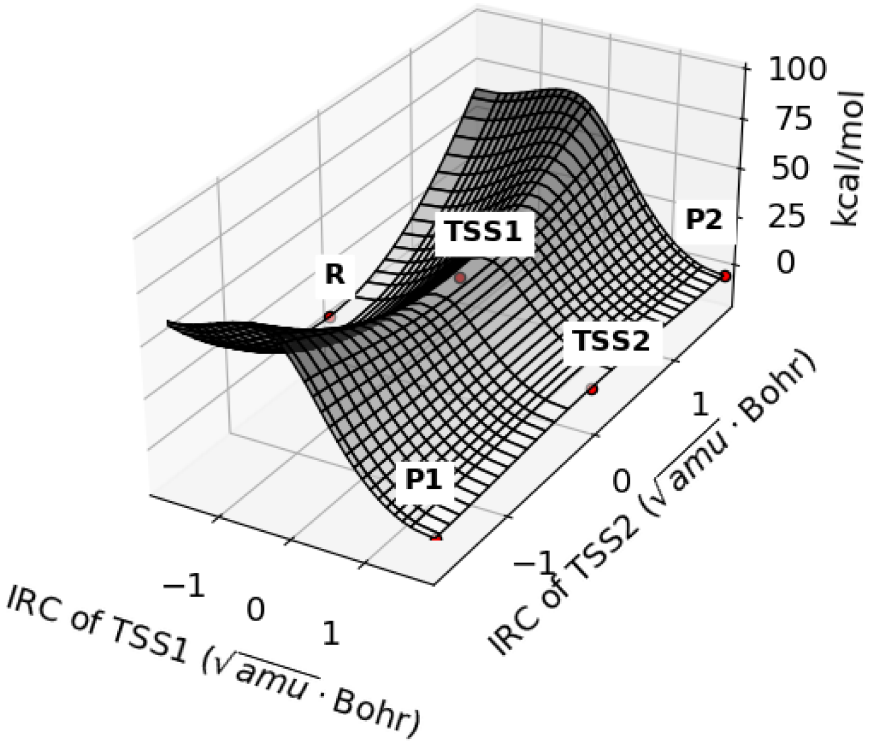

(b)

Figure 3: PESs for methoxy radical isomerization. (a) 2D contour PES. (b) 3D hypersurface.

Hessian eigenvector to force the reaction path follows the ridge, we use the first Hessian eigenvector of **TSS2**; $\mathbf{L}_1^{\mathbf{TSS2}}$, to reduce the computational cost based on this parallel property.

A surface for the same methoxy isomerization constructed previously using empirically chosen geometric parameters for the two dimensions is shown in the Figure 3 of Ref. 29. In their work, the two dimensions were defined from internal coordinates of the system. One dimension was an angle related to the migration of H4. Another dimension consisted of a combination of two dihedral angles defined with two dummy atoms. The central region of their 2D-PES is very similar to the PES we constructed (Figure 3a) even though the definition of two dimensions are different. For the normal coordinate with one and only one negative eigenvalue of **TSS1**, the dominant element is the motion of the transferring proton with a 96% contribution. For **TSS2**, the dominant elements correspond to C−O bond rotation. Nevertheless, for all symmetric PTSBs with given **TSS1** and **TSS2**, our approach is applicable without advanced knowledge (or intuition) of important geometric parameters.

3.2 Asymmetric PTSBs: net C–C insertion for nitrenes

The reaction with an asymmetric PTSB to which we applied our methods is shown in Scheme 2, a serious of reactions involving net C-C insertion for nitrenes, previously designed to have a PTSB.[41] We retained the nomenclature from the previous work ('**NCHn**') for consistency, with all structures studied defined in Table 1 and Scheme 2. All stationary points have C_1 symmetry, and thus, bifurcations must be asymmetric.

It has been demonstrated that an IRP with a shoulder may indicate that a PTSB is present.[1,48] All five **NCHn** systems discussed here have shoulders along the IRP for corresponding **TSS1**s. All of these IRPs end at the local minima corresponding to **P2**s.[41] The second TSS interconverts **P1** and **P2** via a dyotropic rearrangement.[64–69]

In Figure 2, all the 2D-PES for the five **NCHn** systems were included. In these surfaces,

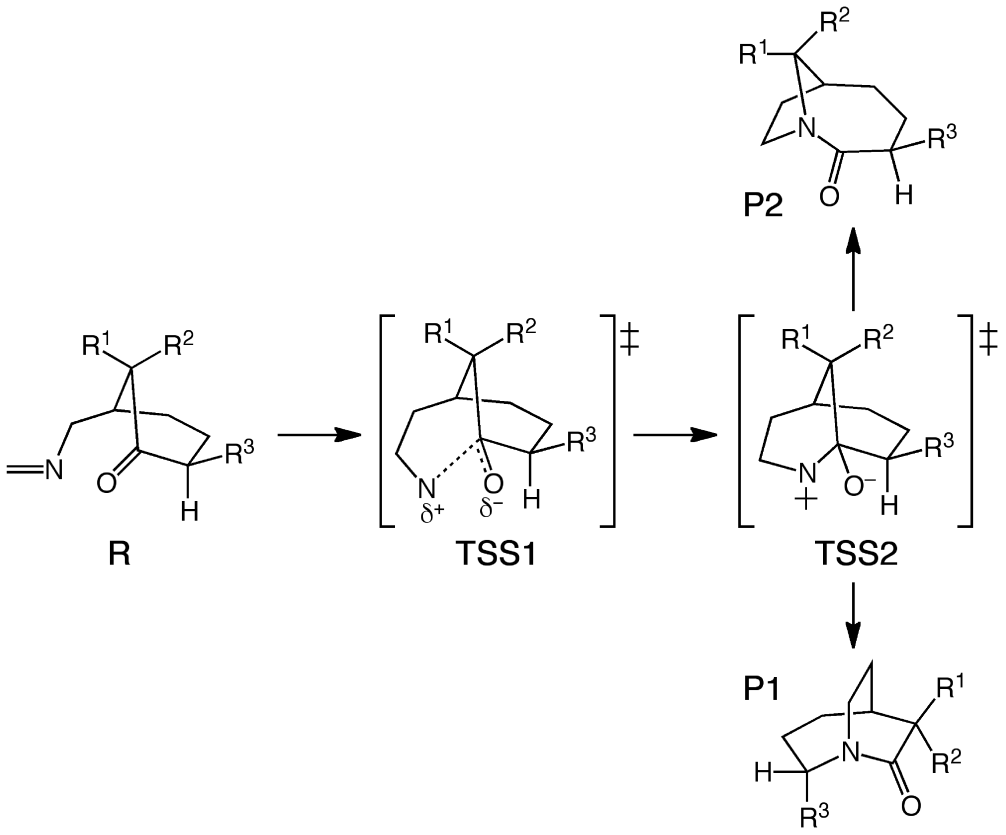

Scheme 2: Stationary points involved in NCHn systems, n = 1 – 5. Both products (**P1**/**P2**) are bicyclic molecules, and **P1** is [3,2,2] and **P2** is [4,2,1].

Table 1: Substituents on **NCH1** - **NCH5**.

	Substituents
NCH1	R^1=H, R^2=H, R^3=H
NCH2	R^1=F, R^2=H, R^3=H
NCH3	R^1=H, R^2=F, R^3=H
NCH4	R^1=H, R^2=H, R^3=F
NCH5	R^1=CF_3, R^2=H, R^3=H

Table 2: 2D-PESs for reactions of **NCH1** to **NCH5** with asymmetric PTSBs, along with zoom-ins of their **VRI** regions (i.e., expansions of regions in red boxes) with color coded energy. Energies are shown in kcal^{-1}mol relative to reactants.

	NCH1	**NCH2**	**NCH3**
2D-PES	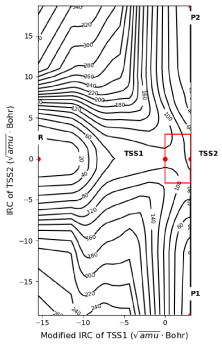	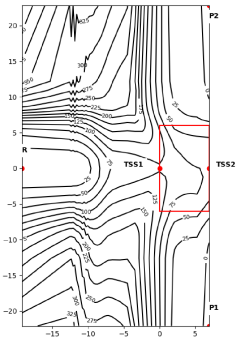	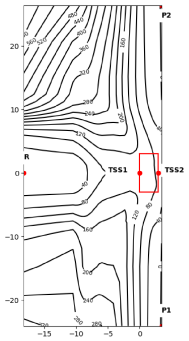
VRI region	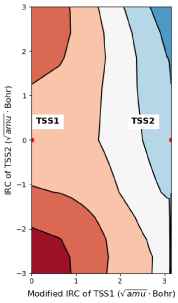	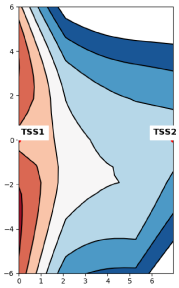	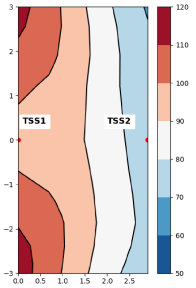
	NCH4	**NCH5**	
2D-PES	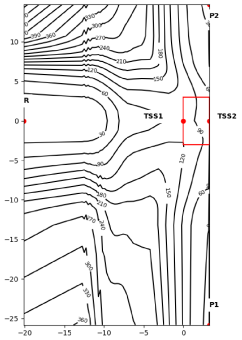	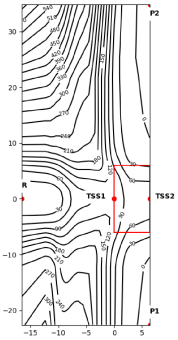	
VRI region	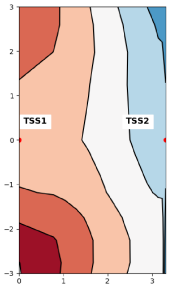	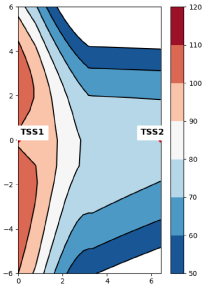	

the two dimensions/reaction coordinates are defined as follows. The x-axis corresponds to a modified IRP for **TSS1**, in which part of the IRP (**R** $\rightarrow$ **TSS1**) is joined with an artificial reaction coordinate (**TSS1** $\rightarrow$ **TSS2**), with our approached in Section 3.2. The y-axis corresponds to the IRP for **TSS2** (**P2** $\rightarrow$ **TSS2** $\rightarrow$ **P1**). On the scale of these plots, the **VRI** region is relatively small, with short distance along the x direction, and this characteristic should affect dynamic behavior, leading to the observed selectivity. The surfaces in the **VRI** regions tilt clearly toward **P2**for **NCH1**-**NCH4**, suggesting that the dominant product is likely to be **P2**. This simple prediction, which was facilitated by examination ofour 2D-PESs, and it was consistent to the observation in dynamics trajectories simulations with **P2** formed in 96%, 73%, 84%, 99% of trajectories for **NCH1**-**NCH4**, respectively.[41] A relatively symmetric 2D-PES is observed for **NCH5** and little selectivity is observed in dynamics simulations: 49% **P1** and 51% **P2**. While resonable, and potentially correct, arguments were made in the previous work to rationalize the selectivity observed in dynamics simulations,[41] tilting of the **VRI** was not discussed, since 2D-PESs of the type described here were not available at the time of publication.

In Figure 4, we showed the results of trajectory mapping. If such trajectory mapping is carried out for particular time intervals, the amount of time spent in the **VRI** region – unambiguously visible in our PES plots – can be accessed. We took **NCH1** as an example, and included such time course in Figure 5. 96 % trajectories leads to **P1** are red, and the other 4 % leads to **P2** are blue. It is seen that, red trajectories of **P1** stay longer near **VRI** region which resulting minor product. Doing so for **NCH1**-**NCH4** indicates that trajectories for **NCH5** spend more time in the **VRI** region on average than do trajectories for other systems (see Supporting Information for details), putting the proposal that the product selectivity can be modulated by lifetime in the **VRI** region in Ref. 41 on firmer footing.

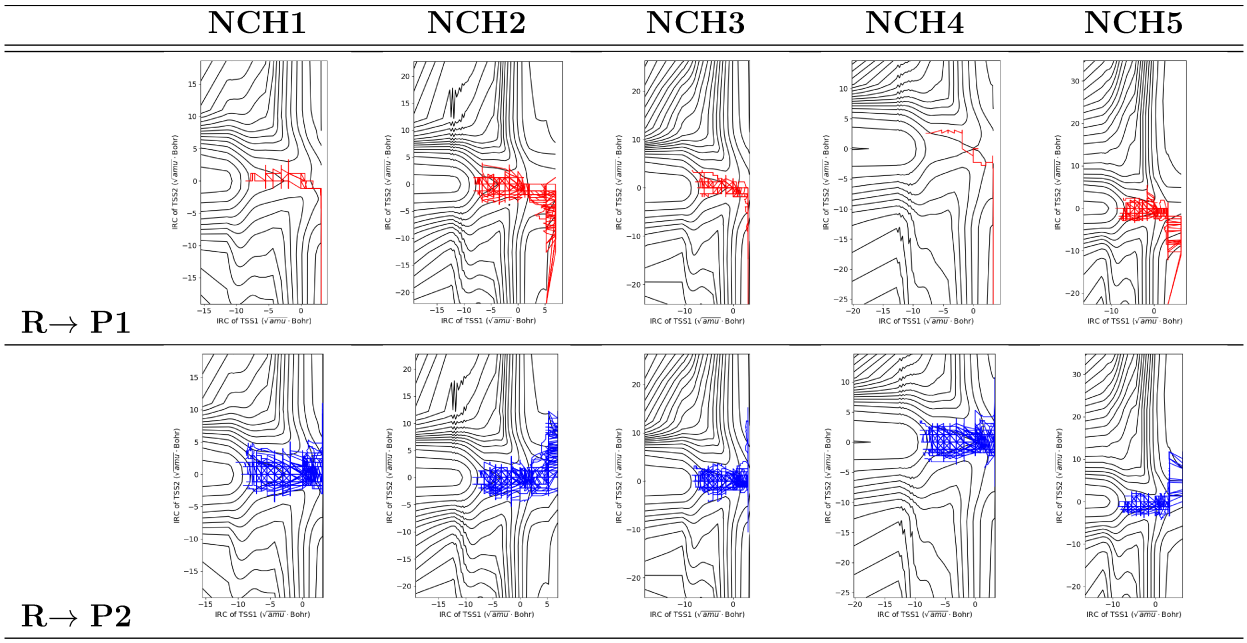

Figure 4: Direct dynamics trajectories mapped onto numerical 2D-PES for **NCH1**-**NCH5**.

4 Conclusions

In this work, we describe two approaches for generating 2D-PESs for both symmetric and asymmetric PTSBs. A reaction with a symmetric PTSB has an ambimodal TSS that has an IRP leading to a secondary TSS. In this case the two IRPs can be used as the two coordinates to form a 2D-PES. In a reaction with an asymmetric PTSB, we generated an artificial reaction path (ARP) that connects the ambimodal TSS to the secondary TSS. The first coordinate for our 2D-PES is the combination of part of the IRP of the ambimodal TSS and the ARC, and the second coordinate is the IRP of the secondary TSS. In order to connect the behavior of trajectories to the shape of our 2D-PESs, we developed an approach to map BOMD trajectories onto our surfaces. Reactions with asymmetric PTSBs have a tilted topography which is clear visualized in our PESs, and we show that this tilting correlates with the product selectivity observed from dynamic simulations.

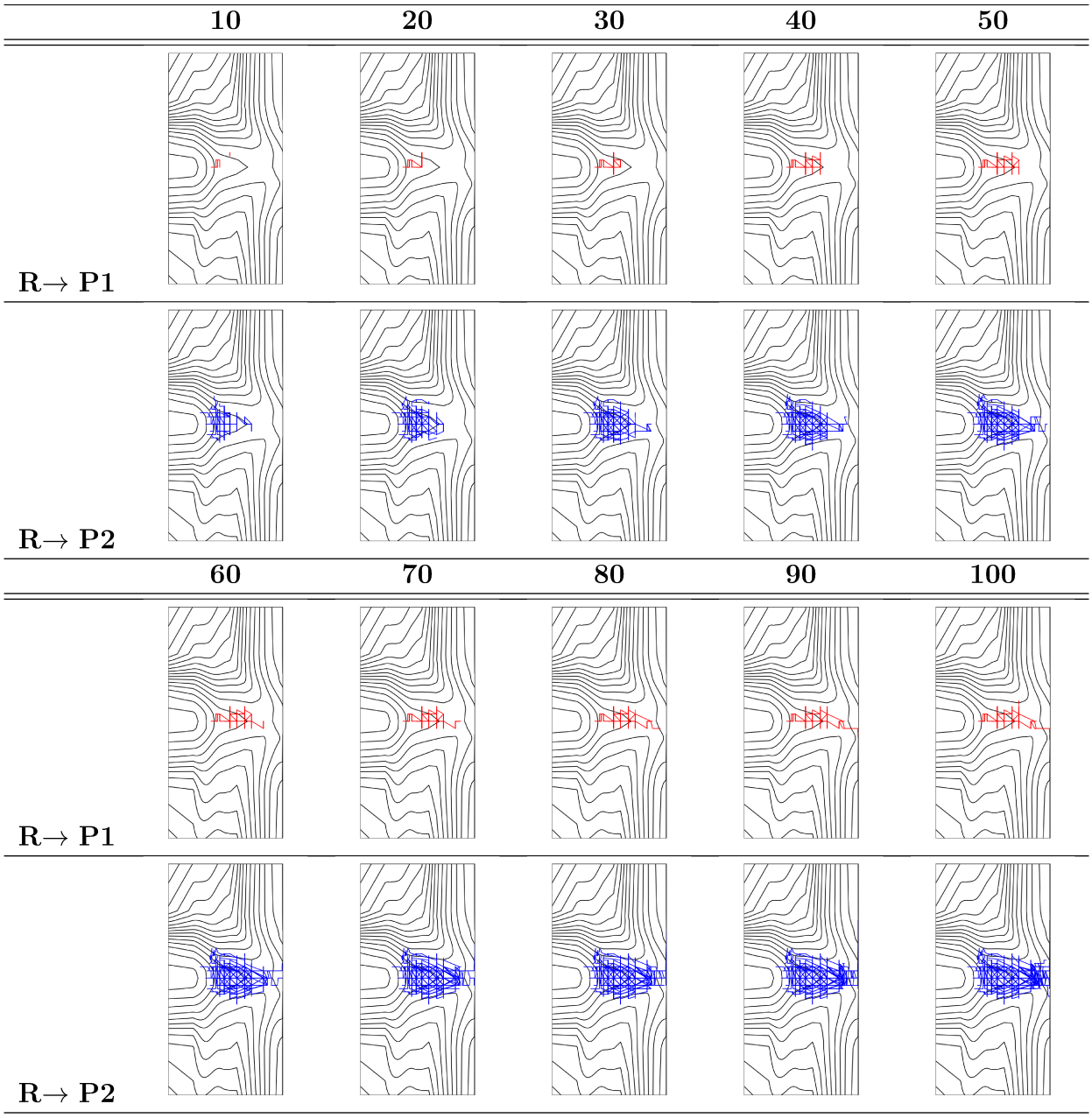

Figure 5: **NCH1**'s direct dynamics trajectories mapped onto numerical 2D-PES hypersurfaces with time evolution. Unit: fs.

5 Acknowledgments

The authors acknowledge Dr. Chun-I Wang, Dr. Lee-Ping Wang and Dr. Renan Borsoi Campos for helpful discussion on revising the manuscript, and problem of rotation of trajectories and dynamic simulations of asymmetric PTSBs, respectively. CPH and HHC

acknowledge support from Academia Sinica Investigator award (AS-IA-106-M01) and the Ministry of Science and Technology of Taiwan (project 105-2113-M-001-009-MY4). HHC is also supported by project 107-2917-I-002-004 from the Ministry of Science and Technology of Taiwan. Support from the US National Science Foundation (CHE-1565933 and CHE-030089 [XSEDE]) to DJT is greatfully acknowledged.

References

(1) Ess, D. H.; Wheeler, S. E.; Iafe, R. G.; Xu, L.; Celebi-Olçüm, N.; Houk, K. N. Bifurcations on Potential Energy Surfaces of Organic Reactions. *Angew. Chem. Int. Ed. Engl.* **2008**, *47*, 7592–7601.

(2) Hare, S. R.; Tantillo, D. J. Post-Transition State Bifurcations Gain Momentum – Current State of the Field. *Pure Appl. Chem.* **2017**, *89*, 679–698.

(3) Martín-Sómer, A.; Yáñez, M.; Hase, W. L.; Gaigeot, M.-P.; Spezia, R. Post-Transition State Dynamics in Gas Phase Reactivity: Importance of Bifurcations and Rotational Activation. *J. Chem. Theory Comput.* **2016**, *12*, 974–982.

(4) Mandal, N.; Datta, A. Dynamical Effects along the Bifurcation Pathway Control Semibullvalene Formation in Deazetization Reactions. *J. Phys. Chem. B* **2018**, *122*, 1239–1244.

(5) Hong, Y. J.; Tantillo, D. J. Biosynthetic Consequences of Multiple Sequential Post-Transition State Bifurcations. *Nat. Chem.* **2014**, *6*, 104–111.

(6) Cane, D. E. Enzymic Formation of Sesquiterpenes. *Chem. Rev.* **1990**, *90*, 1089–1103.

(7) Christianson, D. W. Structural Biology and Chemistry of the Terpenoid Cyclases. *Chem. Rev.* **2006**, *106*, 3412–3442.

(8) Tantillo, D. J. *Applied Theoretical Organic Chemistry*; WORLD SCIENTIFIC (EUROPE), 2018.

(9) Collins, P.; Carpenter, B. K.; Ezra, G. S.; Wiggins, S. Nonstatistical Dynamics on Potentials Exhibiting Reaction Path Bifurcations and Valley-Ridge Inflection Points. *J. Chem. Phys.* **2013**, *139*, 154108.

(10) Miller, W. H.; Handy, N. C.; Adams, J. E. Reaction Path Hamiltonian for Polyatomic Molecules. *J. Chem. Phys.* **1980**, *72*, 99.

(11) Kraka, E.; Wu, A.; Cremer, D. Mechanism of the Diels-Alder Reaction Studied with the United Reaction Valley Approach: Mechanistic Differences Between Symmetry-Allowed and Symmetry-Forbidden Reactions. *J. Phys. Chem. A* **2003**, *107*, 9008–9021.

(12) Kraka, E.; Cremer, D. Computational Analysis of the Mechanism of Chemical Reactions in Terms of Reaction Phases: Hidden Intermediates and Hidden Transition States. *Acc. Chem. Res.* **2010**, *43*, 591–601.

(13) Kraka, E. Reaction Path Hamiltonian and the Unified Reaction Valley Approach. *Wiley Interdiscip. Rev. Comput. Mol. Sci.* **2011**, *1*, 531–556.

(14) Quapp, W. Reduced Gradient Methods and Their Relation to Reaction Paths. *J. Theor. Comput. Chem.* **2003**, *02*, 385–417.

(15) Quapp, W.; Hirsch, M.; Heidrich, D. Following the Streambed Reaction on Potential-Energy Surfaces: a New Robust Method. *Theor. Chim .Acta.* **2000**, *105*, 145–155.

(16) Baker, J.; Gill, P. M. W. An Algorithm for the Location of Branching Points on Reaction Paths. *J. Comput. Chem.* **1988**, *9*, 465–475.

(17) Minyaev, R. M.; Wales, D. J. Gradient Line Reaction Path of HF Addition to Ethylene. *Chem. Phys. Lett.* **1994**, *218*, 413–421.

(18) Maeda, S.; Morokuma, K. Finding Reaction Pathways of Type A + B → X: Toward Systematic Prediction of Reaction Mechanisms. *J. Chem. Theo. Comput.* **2011**, *7*, 2335–2345.

(19) Maeda, S.; Harabuchi, Y.; Ono, Y.; Taketsugu, T.; Morokuma, K. Intrinsic Reaction Coordinate: Calculation, Bifurcation, and Automated Search. *Int. J. Quantum. Chem.* **2015**, *115*, 258–269.

(20) Tsutsumi, T.; Ono, Y.; Arai, Z.; Taketsugu, T. Visualization of the Intrinsic Reaction Coordinate and Global Reaction Route Map by Classical Multidimensional Scaling. *J. Chem. Theory Comput.* **2018**, *14*, 4263–4270.

(21) Müller, K. Reaction Paths on Multidimensional Energy Hypersurfaces. *Angew. Chem. Int. Ed. Engl.* **1980**, *19*, 1–13.

(22) Silver, D. M. Character of the Least-Energy Trajectory near the Saddle-Point on H_3 Potential Surfaces. *J. Chem. Phys.* **1972**, *57*, 586–587.

(23) Fukui, K. Formulation of the Reaction Coordinate. *J. Phys. Chem.* **1970**, *74*, 4161–4163.

(24) Quapp, W. How Does a Reaction Path Branching take Place? A Classification of Bifurcation Events. *J. Mol. Struct.* **2004**, *695-696*, 95–101.

(25) Hare, S. R.; Bratholm, L. A.; Glowacki, D. R.; Carpenter, B. K. Low Dimensional Representations along Intrinsic Reaction Coordinates and Molecular Dynamics Trajectories using Interatomic Distance Matrices. *Chemical Science* **2019**,

(26) Kumeda, Y.; Taketsugu, T. Isotope Effect on Bifurcating Reaction Path: Valley–Ridge Inflection Point in Totally Symmetric Coordinate. *J. Chem. Phys.* **2000**, *113*, 477–484.

(27) Quadrelli, P.; Romano, S.; Toma, L.; Caramella, P. Merging and Bifurcation of 4+2 and 2+4 Cycloaddition Modes in the Rrchetypal Dimerization of Butadiene. A Case of

Competing Bispericyclic, Pericyclic and Diradical Paths. *Tetrahedron Lett.* **2002**, *43*, 8785–8789.

(28) Quadrelli, P.; Romano, S.; Toma, L.; Caramella, P. A Bispericyclic Transition Structure Allows for Efficient Relief of Antiaromaticity Enhancing Reactivity and Endo Stereoselectivity in the Dimerization of the Fleeting Cyclopentadienone. *J. Org. Chem.* **2003**, *68*, 6035–6038.

(29) Lasorne, B.; Dive, G.; Lauvergnat, D.; Desouter-Lecomte, M. Wave Packet Dynamics Along Bifurcating Reaction Paths. *J. Chem. Phys.* **2003**, *118*, 5831–5840.

(30) Celebi-Olçüm, N.; Ess, D. H.; Aviyente, V.; Houk, K. N. Lewis Acid Catalysis Alters the Shapes and Products of Bis-Pericyclic Diels-Alder Transition States. *J. Am. Chem. Soc.* **2007**, *129*, 4528–4529.

(31) Xue, X.-S.; Jamieson, C. S.; Garcia-Borràs, M.; Dong, X.; Yang, Z.; Houk, K. N. An Ambimodal Trispericyclic Transition State and Dynamic Control of Periselectivity. *J. Am. Chem. Soc.* **2019**, *141*, 1217–1221.

(32) Ramquet, M.-N.; Dive, G.; Dehareng, D. Critical Points and Reaction Paths Characterization on a Potential Energy Hypersurface. *J. Chem. Phys.* **2000**, *112*, 4923–4934.

(33) Quapp, W.; Hirsch, M.; Heidrich, D. Bifurcation of Reaction Pathways: the Set of Valley Ridge Inflection Points of a Simple Three-Dimensional Potential Energy Surface. *Theor. Chim .Acta.* **1998**, *100*, 285–299.

(34) Valtazanos, P.; Ruedenberg, K. Bifurcations and Transition States. *Theor. Chim. Acta.* **1986**, *69*, 281–307.

(35) Quapp, W.; Hirsch, M.; Heidrich, D. An Approach to Reaction Path Branching Using Valley-Ridge Inflection Points of Potential-Energy Surfaces. *Theor. Chim .Acta.* **2004**, *112*, 40–51.

(36) Valtazanos, P.; Elbert, S. T.; Xantheas, S.; Ruedenberg, K. The Ring Opening of Cyclopropylidene to Allene: Global Features of the Reaction Surface. *Theor. Chim. Acta.* **1991**, *78*, 287–326.

(37) Wales, D. J. Potential Energy Surfaces and Coordinate Dependence. *J. Chem. Phys.* **2000**, *113*, 3926–3927.

(38) Shaik, S.; Danovich, D.; Sastry, G. N.; Ayala, P. Y.; Schlegel, H. B. Dissociative Electron Transfer, Substitution, and Borderline Mechanisms in Reactions of Ketyl Radical Anions. Differences and Difficulties in their Reaction Paths. *J. Am. Chem. Soc.* **1997**, *119*, 9237–9245.

(39) Oyola, Y.; Singleton, D. A. Dynamics and the Failure of Transition State Theory in Alkene Hydroboration. *J. Am. Chem. Soc.* **2009**, *131*, 3130–3131.

(40) Heidrich, D. *The Reaction Path in Chemistry: Current Approaches and Perspectives*; Springer Netherlands: Dordrecht, 1995; pp 11–38.

(41) Campos, R. B.; Tantillo, D. J. Designing Reactions with Post-Transition-State Bifurcations: Asynchronous Nitrene Insertions into C–C σ Bonds. *Chem.* **2019**, *5*, 227–236.

(42) Hare, S. R.; Tantillo, D. J. Cryptic Post-Transition State Bifurcations that Reduce the Efficiency of Lactone-Forming Rh-Carbenoid C-H Insertions. *Chem. Sci.* **2017**, *8*, 1442–1449.

(43) Duarte, F.; Gronert, S.; Kamerlin, S. C. L. Concerted or Stepwise: How Much Do Free-Energy Landscapes Tell Us about the Mechanisms of Elimination Reactions? *J. Org. Chem.* **2014**, *79*, 1280–1288.

(44) Quapp, W.; Schmidt, B. An Empirical, Variational Method of Approach to Unsymmetric Valley-Ridge Inflection Points. *Theor. Chem. Acc.* **2011**, *128*, 47–61.

(45) Wilson, E. B. E. B.; Decius, J. C.; Cross, P. C. *Molecular Vibrations: The Theory of Infrared and Raman Vibrational Spectra*; Dover Publications: New York, 1980.

(46) Taketsugu, T.; Tajima, N.; Hirao, K. Approaches to Bifurcating Reaction Path. *J. Chem. Phys.* **1996**, *105*, 1933–1939.

(47) Kabsch, W. A Discussion of the Solution for the Best Rotation to Relate Two Sets of Vectors. *Acta. Cryst. A* **1978**, *34*, 827–828.

(48) Hare, S. R.; Tantillo, D. J. Dynamic Behavior of Rearranging Carbocations - Implications for Terpene Biosynthesis. *Beilstein J. Org. Chem.* **2016**, *12*, 377–390.

(49) Ussing, B. R.; Hang, C.; Singleton, D. A. Dynamic Effects on the Periselectivity, Rate, Isotope Effects, and Mechanism of Cycloadditions of Ketenes with Cyclopentadiene. *J. Am. Chem. Soc.* **2006**, *128*, 7594–7607.

(50) Sun, L.; Hase, W. L. In *Reviews in computational chemistry*; Lipkowitz, K. B., Larter, R., Cundari, T. R., Eds.; Reviews in computational chemistry; John Wiley & Sons, Inc.: Hoboken, NJ, USA, 2003; pp 79–146.

(51) Hase, W. L.; Kihyung Song,; Gordon, M. S. Direct Dynamics Simulations. *Comput. Sci. Eng.* **2003**, *5*, 36–44.

(52) Peslherbe, G. H.; Wang, H.; Hase, W. L. In *Advances in Chemical Physics: Monte Carlo Methods in Chemical Physics*; Prigogine, I., Rice, S. A., Eds.; Advances in chemical physics; John Wiley & Sons, Inc.: Hoboken, NJ, USA, 1999; pp 171–201.

(53) Tsutsumi, T.; Harabuchi, Y.; Ono, Y.; Maeda, S.; Taketsugu, T. Analyses of Trajectory on-the-fly Based on the Global Reaction Route Map. *Phys. Chem. Chem. Phys.* **2018**, *20*, 1364–1372.

(54) Frisch, M. J.; Trucks, G. W.; Schlegel, H. B.; Scuseria, G. E.; Robb, M. A.; Cheeseman, J. R.; Scalmani, G.; Barone, V.; Mennucci, B.; Petersson, G. A.; Nakatsuji, H.;

Caricato, M.; Li, X.; Hratchian, H. P.; Izmaylov, A. F.; Bloino, J.; Zheng, G.; Sonnenberg, J. L.; Hada, M.; Ehara, M.; Toyota, K.; Fukuda, R.; Hasegawa, J.; Ishida, M.; Nakajima, T.; Honda, Y.; Kitao, O.; Nakai, H.; Vreven, T.; Montgomery, J. A.; Peralta, J. E.; Ogliaro, F.; Bearpark, M.; Heyd, J. J.; Brothers, E.; Kudin, K. N.; Staroverov, V. N.; Kobayashi, R.; Normand, J.; Raghavachari, K.; Rendell, A.; Burant, J. C.; Iyengar, S. S.; Tomasi, J.; Cossi, M.; Rega, N.; Millam, J. M.; Klene, M.; Knox, J. E.; Cross, J. B.; Bakken, V.; Adamo, C.; Jaramillo, J.; Gomperts, R.; Stratmann, R. E.; Yazyev, O.; Austin, A. J.; Cammi, R.; Pomelli, C.; Ochterski, J. W.; Martin, R. L.; Morokuma, K.; Zakrzewski, V. G.; Voth, G. A.; Salvador, P.; Dannenberg, J. J.; Dapprich, S.; Daniels, A. D.; Farkas,; Foresman, J. B.; Ortiz, J. V.; Cioslowski, J.; Fox, D. J. Gaussian 09, Revision A.02. 2009.

(55) Ditchfield, R.; Hehre, W. J.; Pople, J. A. Self-Consistent Molecular-Orbital Methods. IX. An Extended Gaussian-Type Basis for Molecular-Orbital Studies of Organic Molecules. *J. Chem. Phys.* **1971**, *54*, 724–728.

(56) Becke, A. D. Density-Functional Exchange-Energy Approximation with Correct Asymptotic Behavior. *Phys. Rev. A* **1988**, *38*, 3098–3100.

(57) Lee, C.; Yang, W.; Parr, R. G. Development of the Colle-Salvetti Correlation-Energy Formula into a Functional of the Electron Density. *Phys. Rev. B* **1988**, *37*, 785–789.

(58) Miehlich, B.; Savin, A.; Stoll, H.; Preuss, H. Results Obtained with the Correlation Energy Density Functionals of Becke and Lee, Yang and Parr. *Chem. Phys. Lett.* **1989**, *157*, 200–206.

(59) Becke, A. D. A New Mixing of Hartree–Fock and Local Density-Functional Theories. *J. Chem. Phys.* **1993**, *98*, 1372–1377.

(60) Yanai, T.; Taketsugu, T.; Hirao, K. Theoretical Study of Bifurcating Reaction Paths. *J. Chem. Phys.* **1997**, *107*, 1137–1146.

(61) Powers, D. E.; Pushkarsky, M. B.; Miller, T. A. Rovibronic Analysis of the Laser Induced Fluorescence Excitation Spectrum of the Jet-Cooled Methoxy Radical. *J. Chem. Phys.* **1997**, *106*, 6863–6877.

(62) Rodger, A.; Schipper, P. E. Symmetry Selection Rules for Reaction Mechanisms. *Chem. Phys.* **1986**, *107*, 329–342.

(63) Harabuchi, Y.; Taketsugu, T. A Significant Role of the Totally Symmetric Valley-Ridge Inflection Point in the Bifurcating Reaction Pathway. *Theor. Chem. Acc* **2011**, *130*, 305–315.

(64) Reetz, M. T. Dyotropic Rearrangements, a New Class of Orbital-Symmetry Controlled Reactions. Type I. *Angew. Chem. Int. Ed. Engl.* **1972**, *11*, 129–130.

(65) Reetz, M. T. Dyotropic Rearrangements, a New Class of Orbital-Symmetry Controlled Reactions. Type II. *Angew. Chem. Int. Ed. Engl.* **1972**, *11*, 130–131.

(66) Reetz, M. Primary and Secondary Orbital Effects in Dyotropic Rearrangements. *Tetrahedron* **1973**, *29*, 2189 – 2194.

(67) Reetz, M. Dyotropic Rearrangements and Related $\sigma - \sigma$ Exchange Processes. *Adv. Organomet. Chem.* **1977**, *16*, 33 – 65.

(68) Fernández, I.; Cossío, F. P.; Sierra, M. A. Dyotropic Reactions: Mechanisms and Synthetic Applications. *Chem. Rev.* **2009**, *109*, 6687–6711, PMID: 19746971.

(69) Gutierrez, O.; Tantillo, D. J. Analogies between Synthetic and Biosynthetic Reactions in Which [1,2]-Alkyl Shifts Are Combined with Other Events: Dyotropic, Schmidt, and Carbocation Rearrangements. *J. Org. Chem.* **2012**, *77*, 8845–8850, PMID: 23006240.

Graphical TOC Entry